Check for updates

View Article Online
View Journal

Catalysis Science & Technology

Accepted Manuscript

This article can be cited before page numbers have been issued, to do this please use: W. Yang, Z. Gao, X. Liu, X. Li, X. Ding and W. Yan, *Catal. Sci. Technol.*, 2018, DOI: 10.1039/C8CY01225C.

This is an Accepted Manuscript, which has been through the Royal Society of Chemistry peer review process and has been accepted for publication.

Accepted Manuscripts are published online shortly after acceptance, before technical editing, formatting and proof reading. Using this free service, authors can make their results available to the community, in citable form, before we publish the edited article. We will replace this Accepted Manuscript with the edited and formatted Advance Article as soon as it is available.

You can find more information about Accepted Manuscripts in the author guidelines.

Please note that technical editing may introduce minor changes to the text and/or graphics, which may alter content. The journal's standard Terms & Conditions and the ethical guidelines, outlined in our author and reviewer resource centre, still apply. In no event shall the Royal Society of Chemistry be held responsible for any errors or omissions in this Accepted Manuscript or any consequences arising from the use of any information it contains.

ROYAL SOCIETY OF CHEMISTRY

rsc.li/catalysis

Please do not adjust margins
View Article Online
DOI: 10.1039/C8CY01225C

Catalysis Science & Technology

ARTICLE

Published on 16 July 2018. Downloaded by University of New England on 7/16/2018 3:22:55 AM.

Single atom iron catalyst with single vacancy graphene-based substrate as a novel catalyst for NO oxidation: A theoretical study

Received 00th January 20xx,
Accepted 00th January 20xx

DOI: 10.1039/x0xx00000x

www.rsc.org/

Weijie Yang, [a] Zhengyang Gao *[a], Xiaoshuo Liu [a], Xiang Li [a], Xunlei Ding *[b] and Weiping Yan [a]

Nitric oxide (NO) emitted from coal-fired power plants has raised global concerns. The catalytic oxidation of NO is a promising technology for NO removal. Due to its high selectivity and high catalytic activity, single atom iron catalyst supported with single vacancy (SV) graphene-based substrate (Fe/SV) may be a promising catalyst for NO oxidation. The adsorption characteristics and reaction mechanisms of NO and O_2 on the surface of Fe/SV were systematically studied through density functional theory calculation. The detailed reaction paths under the reaction mechanism of Langmuir-Hinshelwood, Eley-Rideal and termolecular Eley-Rideal were investigated, and thermodynamic and kinetic analysis were performed to study the effect of reaction temperature on the reaction rate and equilibrium. It is found that there are six different reaction paths which can be divided into two reaction patterns of step-by-step and simultaneous. The minimum activation energy of NO oxidation is only 0.04 eV and Eley-Rideal seems to be the dominant reaction mechanism of NO oxidation in flue gas. The reaction temperature has obvious promoting effect on the reaction rate and inhibitory effect on reaction equilibrium. We hope this research can lay a foundation for further theoretical research of NO oxidation and provide guideline for experimental investigation on NO oxidation.

1. Introduction

Nitrogen oxides (NO_x), including nitric oxide (NO), nitrogen dioxide (NO_2), and nitrous oxide (N_2O), are generally recognized as a major source of air pollution in the world. NO_x can not only cause photochemical smog, acid rain and haze, but also greatly contribute to the formation of secondary aerosol and fine particles [1]. NO_x released from coal-fired power plant is the main anthropogenic emission source, and NO accounts for the largest proportion of NO_x. Therefore, it is imperative to control emissions of NO in coal-fired power plant flue gas.

Selective catalytic reduction with ammonia injection (NH_3-SCR) is the most mature and efficient method for emission reduction of NO_x in coal-fired power plant. Although the emission of NO_x equipped with NH_3-SCR can meet emission standard, there are still some problems in the operation process. In order to obtain high removal efficiency of NO_x, a large amount of ammonia is consumed, which can cause catalyst poisoning [2] and ammonia slipping [3]. In addition, the removal efficiency NO_x through the catalytic reduction of NH_3-SCR under low temperature is relatively low, which may lead the emission of NO_x cannot meet the environmental protection regulation. However, catalytic oxidation, which is capable of converting NO to NO_2, can overcome the shortcomings of NH_3-SCR. After catalytic oxidation of NO to NO_2, NO_2 can be well absorbed by desulphurizing slurry in wet flue gas desulfurization system (WFGD) through utilizing its good water solubility. The technology roadmap of catalytic oxidation of NO can avoid ammonia injection and achieve high NO_x removal efficiency under low temperature. In addition, for NH_3-SCR reaction, the reaction rate can be greatly improved if a part of NO is oxidized to NO_2, because the "fast" NH3-SCR reaction ($4NH_3 + 2NO + 2NO_2 \rightarrow 4N_2 + 6H_2O$) is ten times faster than standard NH3-SCR reaction ($4NH_3 + 4NO + O2 \rightarrow 4N_2 + 6H_2O$) under low temperature [1, 4-6]. Therefore, catalytic oxidation of NO can be a promising technology for NO_x removal. Noble metals, such as Pt and Pd, are the most popular catalysts for catalytic oxidation of NO due to its high activity and stability. However, the high costs of noble metals restrict their application to a great extent. Therefore, developing a high efficient and low cost catalyst can greatly accelerate the promotion of catalytic oxidation technology.

Recently, single atom catalysts (SACs) have rapidly become a hot topic in the field of catalysis and chemical industry due to its high activity and selectivity. Moreover, SACs can also reduce the amount of precious metals and maximize the utilization of precious metals [7]. Chaitanya K. Narula1 et al. applied single Pt atom catalyst supported with θ-Al_2O_3 to catalyze the oxidation of NO, and found that its catalytic oxidation activity can come up to commercial platinum particles catalyst [8]. Mehdi D. Esrafili et al. studied the oxidation mechanism of NO catalyzed by single atom Si catalyst supported with boron-nitride nanotubes, and concluded that the oxidation reaction can take place at room temperature [9], confirming that SACs may be a promising catalyst for catalyze the oxidation of NO.

[a] School of Energy and Power Engineering, North China Electric Power University, Baoding 071003, China. E-mail: gaozhyan@163.com
[b] School of Mathematics and Physics, North China Electric Power University, Beijing 102206, China. E-mail: dingxl@ncepu.edu.cn
Electronic Supplementary Information (ESI) available: [details of any supplementary information available should be included here]. See DOI: 10.1039/x0xx00000x

Catalysis Science & Technology Accepted Manuscript

Please do not adjust margins

View Article Online
DOI: 10.1039/C8CY01225C

Published on 16 July 2018. Downloaded by University of New England on 7/16/2018 3:22:55 AM.

Furthermore, SACs which were synthesized by embedding transition metal atoms in graphene-based substrates (TM/GS) can further reduce the cost of catalyst and keep high catalytic activity [10]. Although, the adsorption of NO and NO_2 on TM/GS have been well researched through the density functional theory (DFT) calculation [11-16], there is limited investigation on catalytic oxidation of NO by TM/GS. Therefore, a theoretical study of the catalytic oxidation mechanism of NO by TM/GS is needed to lay the theoretical foundation for the design and development of highly efficient and low cost catalysts. According to the previous investigations, single atom iron catalyst with single vacancy graphene-based substrate (Fe/SV) has high stability and catalytic activity in the adsorption and catalytic oxidation of CO [17-19]. In addition, our previous study also suggests that Fe/SV has high reaction activity in toxic gas adsorption [20]. Therefore, it is natural to expect that Fe/SV can also exhibit similar catalytic behaviour for NO oxidation.

In this work, we studied the oxidation mechanism of NO by O_2 on the surface of Fe/SV through DFT calculation. First, the adsorption characteristics of NO, O_2 and NO_2 on Fe/SV were investigated to obtain the initial reactants for reaction path calculation. Second, the detailed reaction paths under the reaction mechanism of Langmuir-Hinshelwood (L-H), Eley-Rideal (E-R) and termolecular Eley-Rideal (TER) were explored, and the energy variation of NO oxidation reaction process in different reaction path was calculated to determine the rate-determining step. Third, according to above reaction path analysis, thermodynamic and kinetic analysis were performed to investigate the effect of reaction temperature on the reaction equilibrium constant and reaction rate constant. The calculation results can not only reveal the microscopic mechanism of NO oxidation reaction by O_2 on the surface of Fe/SV, but also prove that single atom iron catalyst with single vacancy graphene-based substrate may be a novel catalyst for NO removal in coal-fired power plant.

2. Calculation method

All DFT calculations with Perdew-Burke-Ernzerhof (PBE) functional and projector augmented wave (PAW) potentials were completed in the Vienna ab initio simulation package (VASP) [21-23]. The method of PAW-PBE has been turned out to be an effective method for the calculation of surface adsorption and reaction [10-17, 24]. According to the magnetism of Fe atom, the effect of spin polarization was considered to acquire the correct ground-state energy [25]. According to the previous research models [15, 16, 26], a 4×4 graphene was selected as graphene-based substrate and a 15 Å vacuum layer was adopted to avoid the interaction among mirror images [15, 27].

In accordance with our previous study [28], the cutoff energy of 500 eV was set up for the plane-wave basis set. Gaussian smearing scheme of σ=0.05 eV was used to describe the occupation of the electronic levels [29]. A 7×7×1 Γ-centered k-point grid was selected for structure optimization calculation, which has been turned out to be reasonable and accurate by our previous studies [28]. In detail, the convergence of structure optimization was selected as 0.02 eV/Å. To obtain more accurate electronic structure, a 15×15×1 Γ-centered k-point grid was adopted for energy calculation.

To locate transition states, a method of combining climbing-image nudged elastic band (CI-NEB) [30] with improved dimer method (IDM) [31] were adopted. In detail, CI-NEB method was applied to roughly locate the structures of transition state with the force convergence of 0.1 eV/Å, and then IDM was applied to accurately locate the structures of transition state with the force convergence of 0.05 eV/ Å. To validate the structures of minima and transition states, vibrational frequency was performed with finite displacements of ± 0.02 Å [28, 32]. At the same time, the zero point energy correction from vibrational frequency was calculated to obtain the accurate system energy. According to the calculation of vibrational frequency, there was only one imaginary frequency in transition state structures, while there was no imaginary frequency in minima structures.

To obtain the adsorption strength between gases and catalyst surface, the adsorption energy (E_{ads}) was calculated according to equation (1).

$$E_{ads} = E_{tot} - E_{gas} - E_{sur} \quad (1)$$

Where E_{tot}, E_{gas} and E_{sur} are the total energy of adsorption systems, gases and catalyst surface, respectively. According to the definition, a negative E_{ads} value represents a stable adsorption interaction [33]. In detail, the zero point correction was added into the adsorption energy.

The energy barrier (E_b) and reaction heat (ΔE) were calculated to describe the property of reaction steps, which can be acquired from equation (2) and (3), respectively.

$$E_b = E_{TS} - E_{IS} \quad (2)$$

$$\Delta E = E_{IM} - E_{IS} \quad (3)$$

Where E_{IS}, E_{IM} and E_{TS} are the energy of initial state, Intermediate and transition state, respectively. Moreover, Bader charge was adopted to quantitatively analyze the relevant electron transfer [34].

Thermodynamic analysis of different reaction patterns was conducted through investigating the equilibrium constants and reaction energies, and it can be acquired through the following equation (4) [35]:

$$\Delta G = G_{FS} - G_{IS} = -RT \cdot \ln K \quad (4)$$

Where G_{IS} and G_{FS} are Gibbs free energy of initial state and final state, J • mol-1； K is equilibrium constant.

In detail, the Gibbs free energy of gas and solid can be obtained according to the equations (5) and (6) [36-38]:

$$G_{gas}(T) = E_{ele} + ZPE + RT - TS \quad (5)$$

$$G_{solid}(T) = E_{ele} + ZPE - TS \quad (6)$$

Where E_{ele} is the electron energy of system in ground-state; T is the temperature; S is the entropy of system obtained from vibrational frequency; ZPE is the zero correction energy.

Kinetic analysis of each reaction step was performed by conventional transition state theory based on equation (7) [35]:

$$k^{TST} = \frac{k_B T}{h} \times \exp\left(\frac{-\Delta G_b}{k_B T}\right) \quad (7)$$

Where k_B is the Boltzmann constant, 8.6173303×10^{-5} eV•K^{-1}; T is the reaction temperature; h is the Planck constant, $6.582119514\times10^{-16}$ eV•s; ΔG_b is the energy barrier in Gibbs energy, eV.

Catalysis Science & Technology Accepted Manuscript

This journal is © The Royal Society of Chemistry 20xx

View Article Online
DOI: 10.1039/C8CY01225C
Journal Name ARTICLE

Published on 16 July 2018. Downloaded by University of New England on 7/16/2018 3:22:55 AM.

3. Results and discussion

3.1 Catalyst model

SACs supported with two-dimensional material can be considered as the ideal catalyst model, and there are many successful researches on TM/GS through DFT. In terms of the stability of catalyst, Fe/GS with single vacancy (Fe/SV) is more stable than that with double vacancy (Fe/DV) from our previous study [28], therefore, Fe/SV was selected as the research model. The optimized structure of Fe/SV is shown in Fig. 1 with key parameters of Fe/SV summarized in Table 1. The graphene-based substrates should confine single Fe atom to avoid migration and aggregation. The adsorption energy of Fe atom on the surface of single vacancy graphene is -7.14 eV which is larger than the adsorption energy on perfect graphene (-1.04 eV [39]) and the cohesive energy of the Fe bulk (-4.28 eV [40]), suggesting that graphene-based substrate can firmly anchor Fe atom. Additionally, from Table 1, the calculated key parameters of Fe/SV research model are well consistent with the literature data, which can guarantee the validity and rationality of this research.

Table 1 The bond length of C and Fe atom (*d*, Å), the height of Fe atom (*h*, Å), the charge of Fe atom (*q*, e) and the adsorption energy of Fe atom (E_{ads}, eV) for Fe/SV.

Systems	*d*(Å)	*h*(Å)	*q*(e)	E_{ads}(eV)
Calculation data	1.76	1.35	0.69	-7.14
Literature data	1.76 [17]	1.36 [41]	0.69 [20]	-7.28 [17]

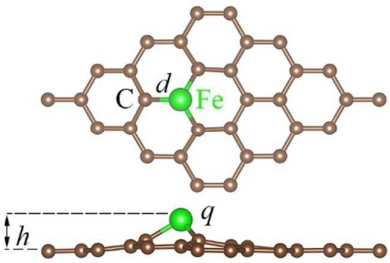

Fig. 1 The geometric structure of Fe/SV.

3.2 Gas adsorption

To obtain the most stable adsorption geometry of reaction gas, different initial configurations were constructed and the optimized adsorption configurations of reaction gases on Fe/SV are shown in Fig. 2. Charge transfer and geometric deformation occur in gas adsorption, and the height variation, charge transfer and adsorption energy were summarized in Table 2. From Table 2, the Fe atom has an obvious uplift in gas adsorption, especially for the coadsorption of O_2 and NO, with an uplift of 0.36 Å. In these adsorption processes, molecules always gain electrons, whereas the Fe atom and graphene-based substrates always lose electrons. In detail, the number of electrons lost by Fe atom are all closely to that lost by graphene-based substrates, indicating that graphene-based substrates can not only anchor the catalyst atom, but also take part in the reaction by donating electrons to gases. The bond length between two oxygen atoms (1.39 Å) is larger than that in gas state (1.21 Å), indicating that oxygen has been activated in the adsorption process. The adsorption energy and bond length of O_2 on Fe/SV (-1.95 eV and 1.39 Å) are larger than that on Au/SV (-1.47 eV and 1.36 Å) [42], which suggests that the activation effect of iron on O_2 is more significant than that of gold. It is expected that the activated oxygen can promote the oxidation reaction of NO. The projected density of states (PDOS) of NO, O_2 and NO_2 adsorption configurations were plotted in Fig. S1. Combining the results of charge transfer and PDOS, we can conclude that two effects of charge transfer and hybridization both take effect in the adsorption of NO and O_2, while charge transfer act as dominant role in the adsorption of NO_2.

Table 2 The height variation of Fe atom (Δ*h*, Å), charge variation (Δ*q*, e) and adsorption energy (E_{ads}, eV) in gas adsorption process.

Gas	Δ*h*(Å)	Δq_{Fe}(e)	Δq_{sub}(e)	Δq_{gas}(e)	E_{ads}(eV)
O	0.09	-0.38	-0.29	0.67	-1.93
O_2	0.12	-0.33	-0.29	0.62	-1.95
NO	0.14	-0.17	-0.15	0.32	-2.15
NO_2	0.09	-0.25	-0.29	0.54	-2.51
2NO	0.32	-0.22	-0.23	0.45	-3.48
O_2+NO	0.36	-0.31	-0.36	0.66	-3.37

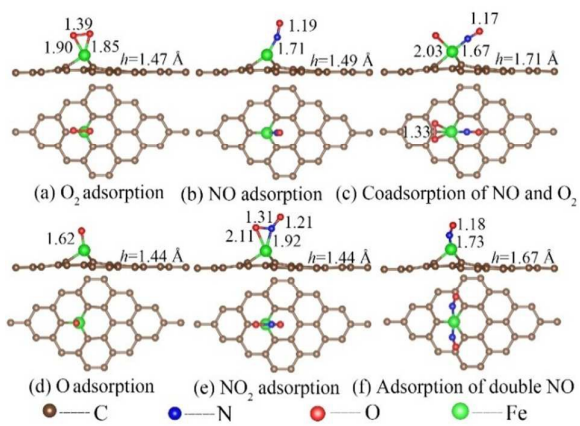

Fig. 2 The adsorption configurations of reaction gases on Fe/SV.

Furthermore, the study of gas adsorption can lay the foundation for initial configuration of reactants in NO oxidation process. Although the adsorption energy of NO (-2.15 eV) is relatively higher than that of O_2 (-1.95 eV), we still consider the situation that NO interacted with adsorbed O_2 on the surface of Fe/SV in E-R reaction mechanism. The volume fraction of O_2 (4 %) is far greater than that of NO (200 ppm) in coal-fired power plant flue gas, hence, it is reasonable to select adsorbed O_2 as initial reactant in E-R reaction mechanism. The adsorption energy of coadsorption is higher than the adsorption energies of O_2 and NO, consequently, L-H reaction mechanism should also be considered. The adsorption energy of double NO molecules is -3.37 eV which is higher than the coadsorption of NO and O_2, indicating that the oxidation reaction of NO may occur in termolecular TER reaction mechanism according to the research of Xu [43]. Therefore, based on the analysis of adsorption

Catalysis Science & Technology Accepted Manuscript

Please do not adjust margins

View Article Online
DOI: 10.1039/C8CY01225C

characteristic of NO and O_2 on the surface of Fe/SV, the reaction mechanisms of L-H, E-R and TER were all considered in the next reaction path analysis.

3.3 Reaction path analysis

3.3.1 L-H reaction mechanism

The reaction path of NO oxidation in L-H reaction mechanism was plotted in Fig. 3 and the corresponding geometric structures, energy barrier (E_b) and reaction heat (ΔE) in reaction process were labelled. In Fig.3, IS, TS and IM stand for initial, transition and intermediate state, respectively. In L-H reaction mechanism, NO and O_2 adsorbed on the surface of Fe/SV at the same time with the exothermic energy being 3.37 eV. The oxidation reaction of NO starts from the coadsorption of NO and O_2 (IS1), and there are two transition state structures and one intermediate state. Firstly, O_2 molecule reversed and stretched to form the NO_2 molecule with an energy barrier of 0.56 eV. The bond length of O_2 molecule increased from 1.33 Å (IS1) to 1.36 Å (TS1), and then elongated to 1.46 Å (IM1). Secondly, NO_2 desorbed from the surface of Fe/SV with an energy barrier of 0.64 eV, and the NO_2 desorption is an exothermic process. According to the energy barriers of each step, the desorption of NO_2 is the rate-determining step in L-H reaction mechanism.

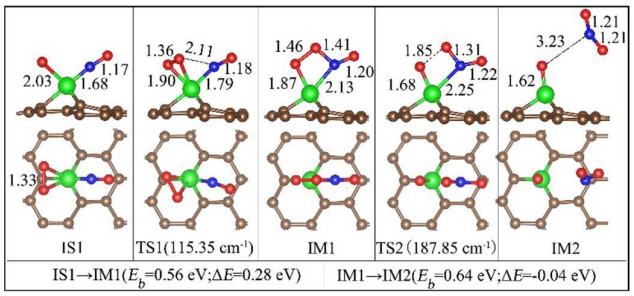

Fig. 3 Top views and side views of reaction configurations in L-H reaction mechanism (Path1).

3.3.2 E-R reaction mechanism

There are two different reaction paths in E-R reaction mechanism in terms of the different attack modes of NO molecule on adsorbed oxygen molecule. The first reaction path of NO oxidation in E-R reaction mechanism was plotted in Fig. 4, and the corresponding geometric structure and energy variation in reaction process were labelled. Firstly, NO molecule attacked the bond between two oxygen atoms adsorbed on the surface of Fe/SV, and formed intermediate with an energy barrier of 0.31 eV. In the attack process, the bond length of O_2 was elongated obviously from 1.39 Å (IS2) to 1.77 Å (TS3) and then increased to 2.17 Å (IM4). Afterwards, desorption of NO_2 from the surface of Fe/SV occurred through N-O bond stretching with a higher energy barrier of 1.10 eV. Similar to L-H reaction mechanism, the desorption process of NO_2 is also the rate-determining step.

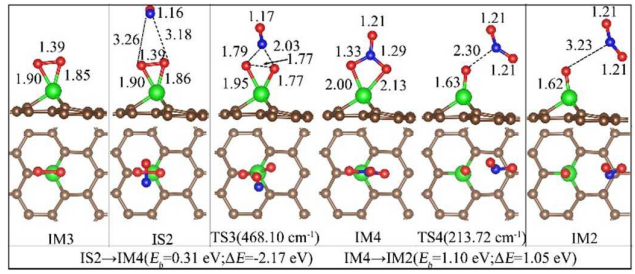

Fig. 4 Top views and side views of reaction configurations in E-R reaction mechanism (Path2).

The second reaction path is that NO molecule attacks one of two oxygen atoms which adsorbed on the surface of Fe/SV, and the reaction path diagram is plotted in Fig. 5. Firstly, NO molecule interacted with one of two oxygen atoms adsorbed on the surface of Fe/SV, and the bond length of oxygen molecule was stretched from 1.39 Å (IM3) to 1.44 Å (IS3). Then, NO_2 molecule desorbed from the surface of Fe/SV meanwhile elongating the bond between two oxygen molecules and shorting the N-O bond between NO molecule and O_2 molecule. Noteworthily, the energy barrier of NO_2 desorption is only 0.02 eV and there is 0.30 eV heat to release in the desorption process, which suggests that the oxidation process of NO in this path is likely to happen at the room temperature.

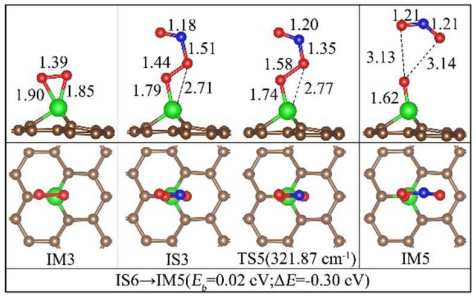

Fig. 5 Top views and side views of reaction configurations in E-R reaction mechanism (Path3).

3.3.3 TER reaction mechanism

Two different reaction paths of TER reaction mechanism were considered with different initial reactants. In the first reaction path, the oxygen molecule attacks two adsorbed NO molecules, and in the second one, two NO molecules attack adsorbed oxygen molecule. The first reaction path was divided into two stages, as shown in Fig. 6 and Fig. 7, respectively. From Fig. 6, oxygen molecule firstly attacked one of two adsorbed NO molecules and the bond length of oxygen molecule was gradually elongated (1.26 Å (IS4) →1.33 Å (TS6) →1.42 Å (IM7)) to form NO_2 with a little energy barrier of 0.23 eV. Subsequently, the generated NO_2 molecule desorbed from the surface of Fe/SV with an energy barrier of 0.70 eV, and there is a relatively large amount of heat (0.97 eV) to release in the process of NO_2 desorption. Noteworthily, a new chemical bond formed by residual O atom of oxygen molecule and C atom of graphene-based substrates, which leaded to the release of relatively large amounts of heat. The reaction rate-

Published on 16 July 2018. Downloaded by University of New England on 7/16/2018 3:22:55 AM.
Catalysis Science & Technology Accepted Manuscript

This journal is © The Royal Society of Chemistry 20xx
Please do not adjust margins

View Article Online
DOI: 10.1039/C8CY01225C

determining step of first stage is NO_2 desorption from the surface of Fe/SV in TER reaction mechanism.

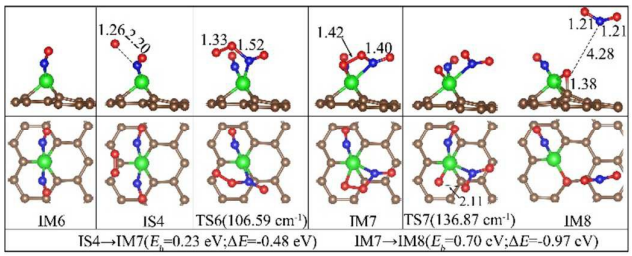

Fig. 6 Top views and side views of reaction configurations in TER reaction mechanism (Path4-1).

For the second stage, as the bond length of N-O gradually decreased (3.05 Å (FS2) → 2.04 Å (TS8) → 1.31Å (IM9)), NO molecule and residual O atom firstly formed NO_2 molecule with a higher energy barrier (1.44 eV). After that, with a little energy barrier (0.14 eV), the bond length of Fe-N gradually increased from 1.92 Å (IM9) to 2.31 Å (TS9), and then stretched to 2.76 Å (IM10). Lastly, NO_2 molecule desorbed from the surface of Fe/SV to complete the cycle of catalytic reaction.

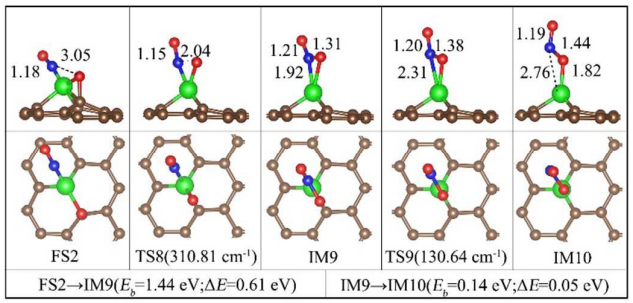

Fig. 7 Top views and side views of reaction configurations in TER reaction mechanism (Path4-2).

The second reaction path of NO oxidation was plotted in Fig. 8, and the corresponding bond length, energy barrier and reaction heat in reaction process were labelled. Two NO molecules attacked the adsorbed oxygen molecule at the same time, and then formed two adsorbed NO_2 molecules with elongating the bond length between two oxygen atoms (1.39 Å(IS5) → 1.89 Å(TS10) → 2.81 Å(IM11)). The energy barrier is 0.92 eV and there is a large amount of heat (1.68 eV) to release in the formation process of NO_2. Subsequently, two adsorbed NO_2 molecules desorbed from the surface of Fe/SV to complete the cycle of catalytic reaction.

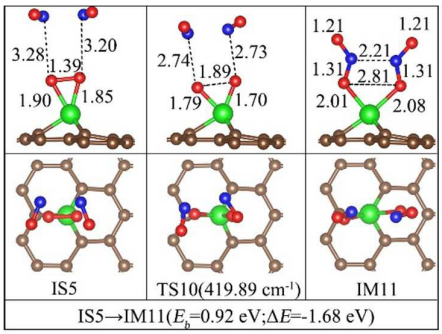

Fig. 8 Top views and side views of reaction configurations in TER reaction mechanism (Path5).

3.3.4 One oxygen atom reaction mechanism

Through above calculation, the reaction paths of NO oxidation in different reaction mechanisms were revealed, and residual oxygen atom was adsorbed on the surface of Fe/SV. To complete the cycle of catalytic reaction, the reaction path of NO oxidation for residual oxygen atom was investigated, as shown in Fig. 9. Firstly, NO molecule adsorbed on the surface of Fe/SV, and formed NO_2 molecule with residual oxygen atom. Then, the bond length between N and Fe was gradually elongated from 1.92 Å (IS6) → 2.30 Å (TS11) → 2.81 Å (IM12), with a small energy barrier (0.13 eV). Lastly, NO_2 molecule desorbed form the surface of Fe/SV.

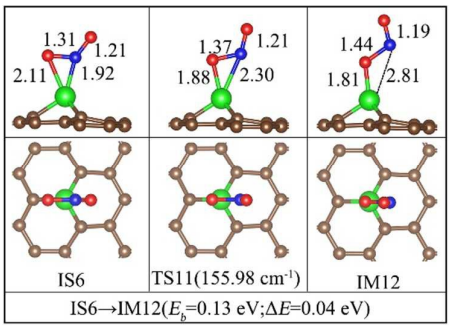

Fig. 9 Top views and side views of reaction configurations in the oxidation of residual oxygen atom (Path6).

3.3.5 Energy variation analysis

In order to compare energy variations under the different paths conveniently, the energy variations of all reaction paths were summarized into a single energy profile, as shown in Fig. 10. In Fig. 10, the zero point of energy was selected as the total energy of reactants. From Fig. 10, there were two main reaction patterns, one is step-by-step and the other is simultaneous. Expect for path5 (TER), the catalytic oxidation of NO on the surface of Fe/SV belongs to step-by-step pattern, which can be divided into two stages according to the generation of NO_2 molecule, and the reaction steps can be described by the equation (8) and (9).

$$NO+O_2 \rightarrow NO_2+O^* \quad (8)$$

$$NO+O^* \rightarrow NO_2 \quad (9)$$

Published on 16 July 2018. Downloaded by University of New England on 7/16/2018 3:22:55 AM.
Catalysis Science & Technology Accepted Manuscript

Please do not adjust margins

View Article Online
DOI: 10.1039/C8CY01225C

Published on 16 July 2018. Downloaded by University of New England on 7/16/2018 3:22:55 AM.

The path5 in TER reaction mechanism belongs to simultaneous pattern, there were two NO_2 molecules generated simultaneously, and the reaction step can be described by the equation (10).

$$2NO+O_2 \rightarrow 2NO_2 \quad (10)$$

For the first stage of NO oxidation in step-by-step pattern, there was a substantial heat (3.06 eV) released and the energy barriers of different reaction paths are all relatively small. The largest energy barrier is 1.10 eV in path2 and the smallest energy barrier is only 0.02 eV in path3, which suggests that the catalytic oxidation of NO in the first reaction path is likely to take place. In the second stage of NO oxidation, there was a large energy barrier (about 2.07 eV) in the desorption process of NO_2, which hinders the cycle of catalytic oxidation. Similarly, there was also a large desorption energy barrier for Path5 in simultaneous pattern. Comparing the energy variations of two stages in the catalytic oxidation of NO, we can conclude that the generation of first NO_2 molecule is relatively easier than the second NO_2. Although the desorption process of second NO_2 needs a relatively large amount of energy, the desorption reaction can still occur in terms of the high temperature of flue gas in coal-fired power plant.

Different from the reaction of CO oxidation on Fe/SV in L-H reaction mechanism [17], the desorption of CO_2 on the surface of Fe/SV is barrierless, while there is an energy barrier of 0.64 eV in NO oxidation. This obvious difference can be understood by comparing the adsorption energy of CO_2 and NO_2 on the surface of Fe/SV. According to above calculation results, the adsorption energy of NO_2 (-2.51 eV) is obviously greater than that of CO_2 (-0.54 eV) [44], indicating that the desorption process of NO_2 from the surface of Fe/SV should be more difficult than that of CO_2. Furthermore, reducing the adsorption energy of NO_2 appropriately can accelerate the oxidation reaction of NO by O_2 on the surface of Fe/SV.

Different from the reaction of CO oxidation on Fe/SV in E-R reaction mechanism [19], the step of NO_2 formation has lower energy barrier (0.31 eV or 0.02 eV) than the reaction of CO oxidation on Fe/SV (0.58 eV), which may be caused by the unpaired electron of NO molecule. Compared with CO molecule, NO molecule has higher reactivity for its unpaired electron, which may promote the adsorption and oxidation of NO on the surface of Fe/SV.

In flue gas, CO and NO both exist at the same time, so it is necessary to further discuss the reaction selectivity between CO oxidation and NO oxidation. Given that adsorption is the first step of chemical reaction, the adsorption characteristic of reaction gas was selected as an indicator to analyse this important issue. In detail, the adsorption configurations and adsorption energies of CO on the surface of Fe/SV were calculated in the same calculation parameter of NO, as shown in Fig. S2. The adsorption configurations of IS1, IS2 and IM6 are the beginning of L-H, E-R and TER reaction mechanism, so we compare the adsorption energies of these adsorption configurations of CO and NO. The adsorption energies of IS1, IS2 and IM6 are -3.37, -0.06 and -3.49 eV, respectively, which are both larger than the adsorption energies of corresponding adsorption configuration of CO (-2.16, -0.02 and -2.54 eV). In addition, the energy barrier of NO oxidation is smaller than that of CO oxidation in the first stage [17, 19]. Consequently, the catalytic oxidation of NO paly a leading role in the first stage.

In the second stage, there was a large energy barrier of the second NO_2 desorption, which hinders the cycle of catalytic reaction. However, the energy barrier in the generation process of second CO_2 molecule is moderate and the desorption of CO_2 is exothermic and thermodynamically favorable [17, 19], which indicates that the oxidation of CO is more likely to happen than NO in the second stage.

Therefore, the oxidation reaction of CO and NO may occur at the same time in the flue gas. In detail, the oxidation of NO may act as a leading role in the first stage due to the higher activity of NO , while the oxidation of CO may play a dominate role in the second stage for its favorable in kinetics and thermodynamics. According to the component of flue gas in coal-fired power plant, the volume fraction of CO (500 ppm) is relatively greater than that of NO (200 ppm). From another point, the CO in fuel gas may promote the oxidation reaction of NO through accelerating the consumption of residual oxygen atom adsorbed on the surface of Fe/SV. The detailed effect of CO on the oxidation of NO should be further investigated in the future research.

Catalysis Science & Technology Accepted Manuscript

This journal is © The Royal Society of Chemistry 20xx

View Article Online
DOI: 10.1039/C8CY01225C
Journal Name ARTICLE

Published on 16 July 2018. Downloaded by University of New England on 7/16/2018 3:22:55 AM.

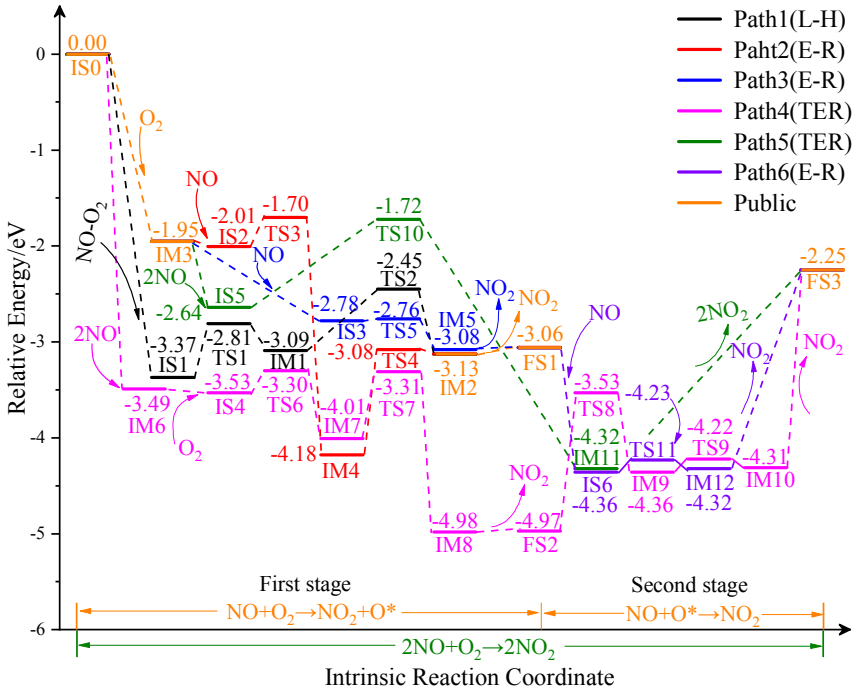

Fig. 10 The energy variations along the intrinsic reaction coordinate for all reaction paths

3.4 Thermodynamic analysis

From above reaction path analysis, the reaction path and energy variations of NO oxidation in different reaction mechanisms can be well understood, and reaction energy (ΔG) and equilibrium constant (K) under different reaction temperatures should be further calculated to obtain the thermodynamic properties of NO oxidation reactions in different reaction paths. Considering the temperature range of fuel gas in coal-fired power plant, the research temperature was selected from 298.15 K to 1000 K. Based on the above analysis of energy variations, the catalytic oxidation of NO can be completed through generating two NO_2 simultaneously or generating NO_2 step by step. Therefore, the thermodynamic analysis was performed focused on these two different patterns (simultaneous and step-by-step). To investigate the effect of temperature on reaction spontaneity and equilibrium, the reaction energies and logarithm of reaction equilibrium constants under different reaction temperature were presented in Fig. 11(a) and (b), respectively.

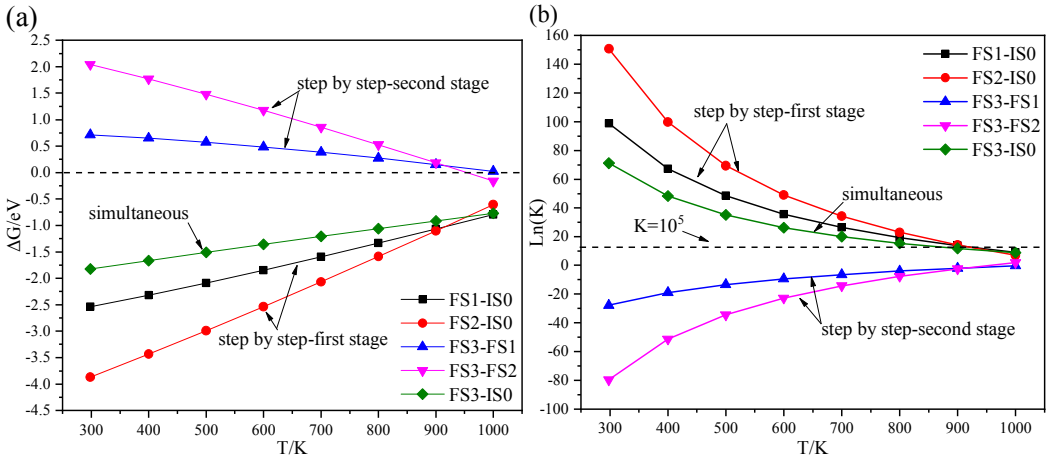

Fig. 11 (a) The reaction variations of different reaction patterns under different reaction temperature. (b) The logarithm of reaction equilibrium constants of different reaction patterns under different reaction temperature.

From Fig. 11(a), the reaction energies of NO oxidation reaction in simultaneous pattern and the first stage of step-by-step pattern are all below zero, which suggests that those NO oxidation reactions can happen spontaneously at the research temperature

Catalysis Science & Technology Accepted Manuscript

Please do not adjust margins

View Article Online
DOI: 10.1039/C8CY01225C

Published on 16 July 2018. Downloaded by University of New England on 7/16/2018 3:22:55 AM.

range. Specifically, the reaction energies of NO oxidation reaction in simultaneous pattern and the first stage of step-by-step pattern increase as the reaction temperature increases, indicating that the reaction temperature has inhibiting effect on spontaneity of NO oxidation reactions. For the second stage of step-by-step pattern, the reaction energies of NO oxidation reaction are all above zero under the research temperature range, so the second stage of NO oxidation in step-by-step pattern cannot take place spontaneously. From Fig. 11(b), the equilibrium constants of NO oxidation reaction in simultaneous pattern and the first stage of step-by-step pattern decrease as the reaction temperature increases, confirming that high reaction temperature can promote the chemical equilibrium of oxidation reaction to the reverse reaction direction. However, the equilibrium constants of NO oxidation in simultaneous pattern and the first stage of step-by-step pattern are all higher than 10^5 in the temperature range from 298.15 K to 800 K[35], suggesting that those NO oxidation reaction in simultaneous pattern and the first stage of step-by-step pattern can be carried out completely and irreversibly.

3.5 Kinetic analysis

Kinetics analysis can acquire kinetic characteristics of different reaction paths, and lay a foundation for further microkinetics calculation. According to the above reaction path analysis, the rate-determining steps of different reaction paths were selected to perform the kinetic analysis. In detail, the rate-determining steps of path1 to path3 were selected as the processes of IM1→IM2, IM4→IM2 and IS3→IM5, respectively. The rate-determining steps of path4 to path 6 were selected as the processes of IM7→IM8 (path4-1), FS2→IM9 (path4-2), IS5→IM11 (path5) and IS6→IM12 (path6), respectively. However, there were large energy barriers for NO_2 desorption in path4-2 to path6 according to the above energy variations (Fig. 10). Therefore, the reaction rate constants of NO_2 desorption should also be considered in the kinetic analysis. To obtain the reaction rate constants of NO_2 desorption (IM10→FS3 (path4-2), IM11→FS3 (path5) and IM12→FS3 (path6)), the method of potential energy surface scanning was adopt to search the energy barrier of NO_2 desorption process, the Fe and O atom were fixed and other atoms allowed to relax freely. The distance between Fe atom and O atom bonded to the Fe atom was gradually increase with a fixed step length of 0.1 Å, and the graph of potential energy surface scanning was plotted in Fig. S3. From Fig. S3, there was no extra energy barrier in the desorption process of NO_2 and we can conclude that the energy barrier of NO_2 desorption is approximately equal to the heat of desorption. Therefore, the reaction rate constants can be calculated according to the equation (7). Due to its complexity of path4 to path6, the logarithm of reaction rate constants of path4 to path6 were plotted in Fig. 12.

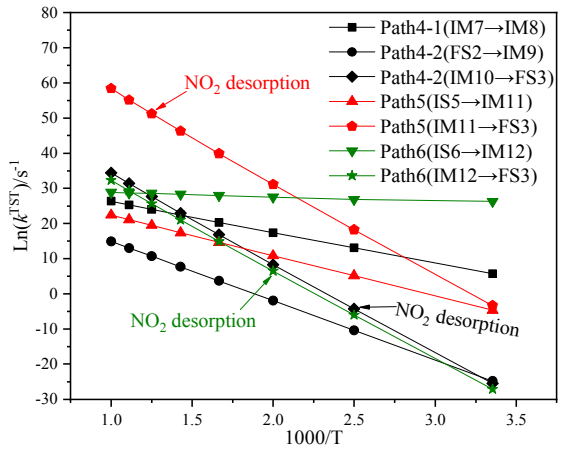

Fig. 12 The logarithm of reaction rate constants of path4 to path6.

From Fig. 12, we can easily identify the rate-determining step through comparing the reaction rate constants, and the rate-determining steps of path4 to path6 should be the process of FS2→IM9, IS5→IM11 and IM12→FS3. It is worth noting that although the desorption process of NO_2 needs a lot of heat, only the rate-determining step of path6 is the process of NO_2 desorption. This may suggest that the reaction temperature has obviously promoting effect on the desorption process of NO_2. At the same time, it also indicates that the desorption processes of products should be paid enough attention in the selection of rate-determining step. Based on the above analysis, the reaction rate constants of rate-determining steps were plotted in Fig. 13.

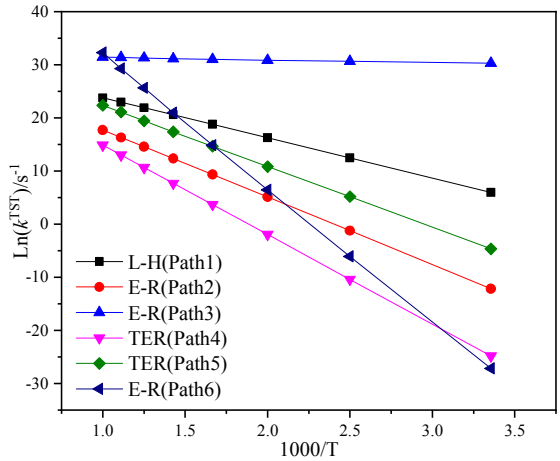

Fig. 13 The logarithm of reaction rate constants of rate-determining steps.

Form Fig. 13, the reaction rate constants of different reaction paths increase with the reaction temperature, which further confirm that the reaction temperature acts as promoting effect on the reaction rate of NO oxidation. In particular, NO oxidation reactions of path3 have high reaction rate constants under the research temperature range. For path6, the oxidation reaction of NO is slow at the low reaction temperature, while the reaction rate constant can be greatly improved at high reaction temperature.

Catalysis Science & Technology Accepted Manuscript

This journal is © The Royal Society of Chemistry 20xx

Please do not adjust margins

View Article Online
DOI: 10.1039/C8CY01225C

Published on 16 July 2018. Downloaded by University of New England on 7/16/2018 3:22:55 AM.

Furthermore, the corresponding Arrhenius parameters of rate-determining steps for different reaction paths, such as pre-exponential factor (*A*) and activation energy (E_a), acquired from linear fitting the reaction rate constants were tabulated in Table 3.

Table 3 The kinetic parameters for different reaction paths.

Paths	E_a (eV)	A (s^{-1})
L-H(Path1)	0.65	4.28×10^{13}
E-R(Path2)	1.09	1.72×10^{13}
E-R(Path3)	0.04	6.73×10^{13}
TER(Path4)	1.46	6.64×10^{13}
TER(Path5)	0.98	4.17×10^{14}
E-R(Path6)	2.17	6.35×10^{24}

From Table 3, there is an obvious difference of reaction paths in activation energy, and the activation energy of NO oxidation reaction ranges from 0.04 eV (path3) to 2.17 eV (path6). According to the temperature level of fuel gas in coal-fired power plant, the above six reaction paths can be relatively easy to happen. Comparing the different reaction paths, the activation energy of NO oxidation reaction in path3 is only 0.04 eV, indicating that the oxidation reaction of NO in path3 can easily take place. The low activation energy of NO oxidation reaction may derive from the activation effect of Fe/SV catalyst on O_2. According to our previous research [20, 28], the activation effect of Fe/GS on O_2 can be further promoted through manufacturing defects and doping on the surface of graphene-based substrates. Therefore, the oxidation reaction of NO by O_2 on the surface of single atom iron catalyst with other different graphene-based substrates should be studied in the future investigation.

Moreover, the NO oxidation reaction of path3 can happen spontaneously at the research temperature range. Therefore, the oxidation reaction of NO by O_2 under the surface of Fe/SV is likely to be carried out mainly through path3. However, the reaction mechanism of E-R and L-H must pass the path6 to complete the cycle of the catalyst and the path6 is the slowest between the six reaction paths, which suggests that the reaction mechanism of E-R may be not the most favorable. Based on the analysis of reaction selectivity, the CO in the flue gas of coal-fired power plant will preferentially interact with the residual oxygen atom adsorbed on the surface of Fe/SV to promote the cycle of catalytic reaction. Therefore, the reaction mechanism of E-R should also be dominant in the flue gas environment.

Compared with the research of literatures [9], the smallest activation energies of NO oxidation by O_2 on the surface of single atom Si catalyst supported with boron-nitride nanotubes is 0.01 eV, which is lower than our calculated activation energy on Fe/SV (0.04 eV). In the view of reaction kinetics, the catalytic oxidation of NO on the surface of single atom Si catalyst is better than that on Fe/SV. However, the oxidation reactions of NO on the surface of single atom Si catalyst are all not favorable in thermodynamics. According to above thermodynamic analysis, the first stage of NO oxidation reaction in step by step pattern can occur spontaneously and irreversibly. Therefore, Fe/SV seems to be a promising catalyst for NO oxidation based on the kinetic and thermodynamic analysis.

4. Conclusions

The adsorption characteristics and reaction mechanism of NO and O_2 on the surface of Fe/SV were systematically studied through DFT calculation. The detail reaction paths under L-H, E-R and TER mechanism were investigated, and thermodynamic and kinetic analysis were performed to consider the effect of reaction temperature on the reaction rate and equilibrium constant. It is found that there are six different reaction paths which can be divided into two patterns of step-by-step and simultaneous. In the first stage of step-by-step patterns, the oxidation reaction of NO can be carried out completely and take place irreversibly and spontaneously in the temperature range from 298.15 K to 800 K, while the second stage is endothermic and cannot occur spontaneously. For the selectivity of CO oxidation and NO oxidation, the oxidation of NO may act as a leading role in the first stage, while the oxidation of CO may play a dominate role in the second stage. The activation energy of NO oxidation ranges from 0.04 eV to 2.17 eV. The minimum activation energy of NO oxidation is only 0.04 eV and Eley-Rideal seems to be the dominant reaction mechanism of NO oxidation in flue gas. Among the six reaction paths, the desorption process of NO_2 is relatively slow in the low reaction temperature. The reaction temperature has obvious promoting effect on the reaction rate and inhibitory effect on reaction equilibrium. Based on the above analysis, we can conclude that Fe/SV seems to be a promising catalyst for NO oxidation.

For further study, the reaction mechanism of NO oxidation with the participation of CO should be investigate. In light of complexity of fuel gas in coal-fired power plant, the effect of SO_2 and H_2O on oxidation reaction of NO will be considered. Given the tunability of Fe/GS, we can regulate the adsorption of O_2 and NO_2 on the surface of Fe/GS by modifying graphene-based substrates to further reduce the energy barrier of NO_2 desorption. Therefore, it may be of interest to investigate the reaction mechanism of NO oxidation on Fe/GS supported with defect and doped graphene-based substrates.

Conflicts of interest

There are no conflicts to declare.

Acknowledgements

This work was supported by the National Natural Science Foundation of China (No. 91545122), Beijing Natural Science Foundation (2182066), Natural Science Foundation of Hebei Province of China (B2018502067), the Fundamental Research Funds for the Central Universities (JB2015RCY03 and 2017XS121) and the foundation of Shanxi Key Laboratory of Clean & High Efficient Combustion and Utilization of Circulating Fluidized Bed (No. SKLCFB-201701). Computational resources from the Lvliang Supercomputer Center were acknowledged.

Notes and references

Catalysis Science & Technology Accepted Manuscript

Please do not adjust margins

View Article Online
DOI: 10.1039/C8CY01225C

Published on 16 July 2018. Downloaded by University of New England on 7/16/2018 3:22:55 AM.

1. Z. Hong, Z. Wang and X. B. Li, *Catal. Sci. Technol*, 2017, **7**, 3440-3452.
2. M. S. Maqbool, A. K. Pullur and H. P. Ha, *Appl. Catal., B,* 2014, **152-153**, 28-37.
3. W. Chen, Z. Qu, W. Huang, X. Hu and N. Yan, *Fuel*, 2016, **166**, 179-187.
4. P. Forzatti, L. Castoldi, I. Nova, L. Lietti and E. Tronconi, *Catal. Today*, 2006, **117**, 316-320.
5. G. Madia, M. Koebel, M. Elsener and A. Wokaun, *Ind. Eng. Chem. Res*, 2002, **41**, 3512-3517.
6. M. Koebel, M. Elsener and G. Madia, *Ind. Eng. Chem. Res*, 2001, **40**, 52-59.
7. X. F. Yang, A. Q. Wang, B. T. Qiao, J. Li, J. Y. Liu and T. Zhang, *Acc. Chem. Res*, 2013, **46**, 1740-1748.
8. C. K. Narula, L. F. Allard, G. M. Stocks and M. Moses-DeBusk, *Sci Rep*, 2014, **4**, 7238.
9. M. D. Esrafili and N. Saeidi, *Superlattices Microstruct*, 2015, **81**, 7-15.
10. B. Bayatsarmadi, Y. Zheng, A. Vasileff and S.-Z. Qiao, *Small*, 2017, **13**, 1700191.
11. M. D. Esrafili, N. Saeidi and L. Dinparast, *Chem. Phys. Lett*, 2017, **687**, 290-296.
12. E. Ashori, F. Nazari and F. Illas, *Phys. Chem. Chem. Phys*, 2017, **19**, 3201-3213.
13. Y. Chen, B. Gao, J. X. Zhao, Q. H. Cai and H. G. Fu, *J. Mol. Model*, 2012, **18**, 2043-2054.
14. Y. Tang, Z. Liu, Z. Shen, W. Chen, D. Ma and X. Dai, *Sens. Actuators, B*, 2017, **238**, 182-195.
15. Y. Tang, W. Chen, C. Li, L. Pan, X. Dai and D. Ma, *Appl. Surf. Sci*, 2015, **342**, 191-199.
16. Y. Lee, S. Lee, Y. Hwang and Y.-C. Chung, *Appl. Surf. Sci*, 2014, **289**, 445-449.
17. Y. Tang, J. Zhou, Z. Shen, W. Chen, C. Li and X. Dai, *RSC Adv.*, 2016, **6**, 93985-93996.
18. L. Wang, Q. Luo, W. Zhang and J. Yang, *J. Hydrogen Energy*, 2014, **39**, 20190-20196.
19. Y. Li, Z. Zhou, G. Yu, W. Chen and Z. Chen, *J. Phys. Chem. C*, 2010, **114**, 6250-6254.
20. Z. Gao, W. Yang, X. Ding, G. Lv and W. Yan, *Appl. Surf. Sci*, 2018, **436**, 585-595.
21. G. Kresse and D. Joubert, *Phys. Rev. B*, 1999, **59**, 1758.
22. G. Kresse and J. Furthmüller, *Comput. Mater. Sci*, 1996, **6**, 15-50.
23. G. Kresse and J. Furthmüller, *Phys. Rev. B*, 1996, **54**, 11169.
24. J. P. Perdew, K. Burke and M. Ernzerhof, *Phys. Rev. Lett*, 1996, **77**, 3865.
25. A. D. Becke and E. R. Johnson, *J. Chem. Phys*, 2005, **122**, 154104.
26. M. Sun, W. Tang, Q. Ren, S. Wang, JinYu, Y. Du and Y. Zhang, *Appl. Surf. Sci*, 2015, **356**, 668-673.
27. L. Ma, J.-M. Zhang, K.-W. Xu and V. Ji, *Appl. Surf. Sci*, 2015, **343**, 121-127.
28. Z. Gao, W. Yang, X. Ding, G. Lv and W. Yan, *Phys. Chem. Chem. Phys*, 2018, **20**, 7333.
29. K. T. Chan, J. B. Neaton and M. L. Cohen, *Phys. Rev. B.*, 2008, **77**.
30. G. Henkelman and H. Jónsson, *J. Chem. Phys*, 2000, **113**, 9978-9985.
31. A. Heyden, A. T. Bell and F. J. Keil, *J. Chem. Phys*, 2005, **123**, 224101.
32. C. Riplinger and E. A. Carter, *J. Phys. Chem. C*, 2015, **119**, 9311-9323.
33. J. Liu, M. A. Cheney, F. Wu and M. Li, *J. Hazard. Mater*, 2011, **186**, 108-113.
34. W. Tang, E. Sanville and G. Henkelman, *J. Phys.: Condens. Matter*, 2009, **21**, 084204.
35. Z. Gao, W. Yang, X. Ding, Y. Ding and W. Yan, *Appl. Therm. Eng*, 2017, **126**, 28-36.
36. K. Reuter and M. Scheffler, *Phys. Rev. B*, 2001, **65**.
37. C. Ling, L. Shi, Y. Ouyang, X. C. Zeng and J. Wang, *Nano Lett*, 2017, **17**, 5133-5139.
38. J. Zhao and Z. Chen, *J. Am. Chem. Soc*, 2017, **139**, 12480-12487.
39. M. Manadé, F. Viñes and F. Illas, *Carbon*, 2015, **95**, 525-534.
40. P. Janthon, S. M. Kozlov, F. Vines, J. Limtrakul and F. Illas, *J. Chem. Theory Comput*, 2013, **9**, 1631-1640.
41. A. V. Krasheninnikov, P. O. Lehtinen, A. S. Foster, P. Pyykko and R. M. Nieminen, *Phys. Rev. Lett*, 2009, **102**, 126807.
42. T. Zhang, Q. Xue, M. Shan, Z. Jiao, X. Zhou, C. Ling and Z. Yan, *J. Phys. Chem. C*, 2012, **116**, 19918-19924.
43. G. Xu, R. Wang, F. Yang, D. Ma, Z. Yang and Z. Lu, *Carbon*, 2017, **118**, 35-42.
44. D. Cortés-Arriagada, N. Villegas-Escobar and D. E. Ortega, *Appl. Surf. Sci*, 2018, **427**, 227-236.

Catalysis Science & Technology Accepted Manuscript

This journal is © The Royal Society of Chemistry 20xx

View Article Online
DOI: 10.1039/C8CY01225C

Published on 16 July 2018. Downloaded by University of New England on 7/16/2018 3:22:55 AM.

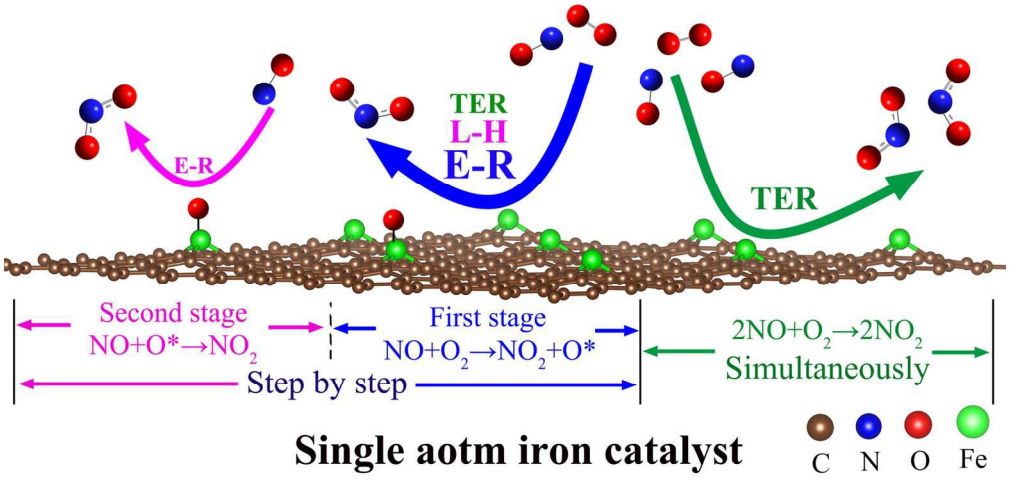

74x37mm (600 x 600 DPI)

Catalysis Science & Technology Accepted Manuscript